

# Time resolved imaging of the non-linear bullet mode within an injection-locked spin Hall nano-oscillator

T. M. Spicer,<sup>1</sup> P. S. Keatley,<sup>1</sup> M. Dvornik,<sup>2</sup> T. H. J. Loughran,<sup>1</sup> A. A. Awad,<sup>2</sup> P. Dürrenfeld,<sup>2</sup> A. Houshang,<sup>2</sup> M. Ranjbar,<sup>2</sup> J. Åkerman,<sup>2,3</sup> V. V. Kruglyak,<sup>1</sup> and R. J. Hicken<sup>1</sup>

<sup>1</sup>*Department of Physics and Astronomy, University of Exeter, EX4 4QL, United Kingdom*

<sup>2</sup>*Department of Physics, University of Gothenburg, 412 96 Gothenburg, Sweden*

<sup>3</sup>*Materials Physics, School of ICT, KTH-Royal Institute of Technology, Electrum 229, 164 40 Kista, Sweden*

Time-resolved scanning Kerr microscopy has been used to image large amplitude precessional magnetization dynamics excited by a DC current within a spin Hall nano-oscillator (SHNO). The SHNO was formed from a 4 micron diameter Py(5 nm)/Pt(6 nm) mesa defined upon a  $Al_2O_3$  substrate, with triangular Au(150 nm) contacts overlaid. Injection of a radio frequency (RF) current was used to phase lock the SHNO to the femtosecond laser. Time resolved imaging revealed a non-linear ‘bullet’ mode with a clear threshold behaviour, that can be separated from the small amplitude Ferromagnetic resonance (FMR) induced by the RF current. The out of plane magnetization component is readily detected by means of the polar magneto optical Kerr effect (MOKE). However images obtained by means of longitudinal MOKE measurements are dominated by an artifact arising from the edges of the Au contacts. As the DC current is increased above threshold, the bullet appears to increase in size, suggesting an increased translational motion. This behaviour may be associated with spreading of the RF spin current away from the centre of the device.

Spin orbit torques are being intensively studied both to understand their physical origin and to realize new applications. Within a nanoscale spin torque oscillator (STO), magnetic auto-oscillations, with frequencies that range from the MHz to GHz regimes, are driven by the spin transfer torque (STT) associated with injection of spin current. The frequency and amplitude of oscillation can be tuned via either an electrical bias current or an applied magnetic field, while the magnetoresistance of the constituent materials leads to the generation of voltage oscillations. Consequently the STO has strong potential for use in magnetic sensing, signal processing, and neuromorphic computing applications [1–3]. High density arrays of STOs can also be envisaged that offer the prospect of increased output power through mutual synchronisation. However it is first necessary to understand the character, localisation and stability of the underlying magnetization dynamics.

While the first STOs exploited spin-polarized current injection, within a spin Hall nano-oscillator (SHNO) the Spin Hall effect (SHE) [4, 5] is used to drive a pure spin current from a heavy metal with large spin-orbit interaction into a ferromagnet layer [6–8]. The de-coupling of charge and spin currents opens up new device geometries, enabling the exploitation of magnetic insulators[9], and in the present study, allows for access of an optical probe to the active region of the device.

The generation of magnetic auto-oscillations requires a critical spin current density to be exceeded. Within the SHNO it is necessary to concentrate the injected charge current within a small region of the heavy metal. This has been achieved by either overlaying thick needle shaped contacts on the heavy metal layer [6, 10–14] or by forming a nanoconstriction within the heavy metal/ferromagnet bilayer[15–20]. SHNOs of both kinds have been

studied by means of Brillouin Light Spectroscopy (BLS), microwave spectroscopy and micro-magnetic simulations. While the spectral characteristics of the dynamics have been explored, the time-evolution of the magnetization has yet to be measured directly.

In the present work, time resolved scanning Kerr microscopy (TRSKM)[21, 22] is used to observe the time dependent magnetization within a SHNO that has been phase locked to an injected radio frequency (RF) current  $I_{RF}$ . Formation of the non-linear ‘bullet’ mode is observed when the injected DC current  $I_{DC}$  exceeds a threshold value. Comparison with micromagnetic simulations shows that the diameter of the bullet is small compared to that of the optical spot. Nevertheless the apparent diameter of the bullet mode is observed to increase with  $I_{DC}$ , suggesting increased translational motion of the bullet.

SHNOs were fabricated by a combination of sputter deposition and electron-beam lithography. A  $4\mu m$  Py(5 nm)/Pt(6 nm) bi-layer disk was first defined, before two triangular Au(150 nm) nanocontacts (NCs), with a tip separation of 200 nm, were overlaid as shown in figure 1a. The device is designed to concentrate electrical current within the Pt layer at the NC tips. Here the charge current is used to generate a spin current, by means of the SHE, that propagates normal to the plane of the device into the Py layer. Once the STT compensates the damping, a self-localized non-linear mode is formed, that has been described as a spin wave bullet. While other modes can be supported within the disk ([14] demonstrates propagating waves when the Py is magnetized normal to the plane), the bullet mode is of particular interest due to its narrow linewidth and tuneable frequency.

Initial microwave electrical measurements exploited the magnetoresistive response of the Py layer. A ground-

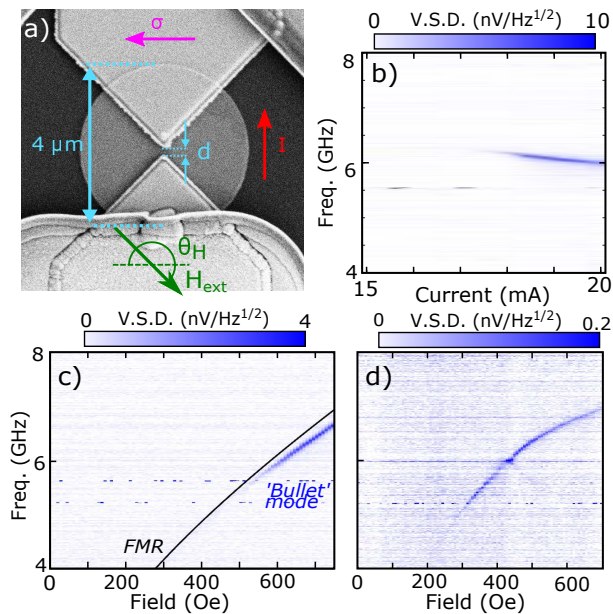


FIG. 1. a) SEM image of a typical SHNO, where  $I$  is the injected current,  $\sigma$  the corresponding spin polarization,  $d$  the NC separation, and  $H$  the magnetic field applied at angle  $\theta_H$ . b) Voltage Spectral Density (VSD) of microwave emission from a SHNO with  $d=240$  nm at fixed magnetic field  $H = 650$  Oe and  $\theta_H = 210^\circ$  for different values of  $I_{DC}$ . c) Emission excited in a SHNO with  $d = 240$  nm for  $I_{DC} = 18$  mA, with magnetic field  $H$  orientated at  $\theta_H = 150^\circ$ . The solid black line shows the field dependence of the FMR frequency obtained from STT-FMR measurements. d) Emission from the device in (c) when  $I_{DC} = 18.5$  mA and  $I_{RF}$  has amplitude of 3.5 mA and frequency of 12 GHz.

signal-ground electrical probe was used to make electrical contact to a selected device and connect it to a bias-tee. The inductive and capacitive arms were used to supply  $I_{DC}$  and  $I_{RF}$  respectively, while the RF signal returned from the device was directed into a spectrum analyzer via a circulator and +24 dB pre-amplifier. TRSKM measurements were performed with a vector-quadrant bridge detector that exploits different magneto-optical Kerr effect (MOKE) geometries to simultaneously detect the three spatial components of the dynamic magnetization and the optical reflectance [23]. For the dynamics to be observed in a stroboscopic fashion, they must be synchronised, via the injected  $I_{RF}$ , to an exact multiple of the 80 MHz laser repetition rate. The phase of  $I_{RF}$  can then be adjusted relative to the laser pulses so that the time evolution of the magnetization dynamics can be observed. Measurements were performed with phase modulation of  $I_{RF}$  to enhance the signal to noise ratio. The laser pulses had 800 nm wavelength, and were focused to a spot of  $\sim 870$  nm FWHM diameter by a microscope objective with 10.1 mm working distance and 0.55 numerical aperture [24].

Microwave electrical measurements were performed to

identify the bullet mode and confirm locking to  $I_{RF}$ . Figure 1b shows the emission from a SHNO for fixed field and increasing  $I_{DC}$ . The onset of emission is observed at  $I_{DC} \sim 18$  mA. The frequency red-shifts with increasing  $I_{DC}$  and emission is still present at  $I_{DC} = 20$  mA. No emission is observed if the sign of either the field  $H$  or  $I_{DC}$  is changed, in agreement with the expected symmetry of the SHE. Figure 1c shows the field and frequency dependence of both the Ferromagnetic Resonance (FMR), determined from separate STT-FMR measurements (consistent with previous work [11, 25]), and the microwave emission. For a given frequency, microwave emission is observed at a field close to but greater than that of the FMR mode. The dependence of the frequency upon  $H$  and  $I_{DC}$  is consistent with previous observations of the bullet mode [13].

Stroboscopic TRSKM measurements require the bullet mode to be synchronised to  $I_{RF}$ . Figure 1d demonstrates that a bullet mode of 6 GHz frequency can be locked to an  $I_{RF}$  of 12 GHz frequency. As  $H$  is varied, the frequency of emission approaches 6 GHz and is ‘pulled’ towards the locking regime. Within this region an increase in output power and reduction in linewidth is observed. Outside this regime an intermodulation mode can be observed, decreasing in frequency with increasing field. A large  $I_{RF}$  of  $\sim 3.5$  mA amplitude was required to achieve even a narrow locking range, which has been attributed to thermal noise enhanced by the spin current [10]. An optically-detected STT-FMR study of similar devices [26] showed that the reactance of the device geometry causes spatial spreading of  $I_{RF}$  that drives FMR within the extended disk. Therefore TRSKM measurements were performed with the frequency of  $I_{RF}$  set to 6 GHz so as to minimise the amplitude required to achieve locking [27].

Figure 2a shows TRSKM images acquired with the bullet mode locked to  $I_{RF}$ , and when  $I_{RF}$  is still present but  $I_{DC} = 0$  mA. In the latter case,  $I_{RF}$  drives the FMR with  $H$  detuned from the line centre. The addition of  $I_{DC}$  leads to additional dynamics in all three magnetic channels. In the polar magnetization channel, localized precession is observed between the NC tips, with a different phase to the dynamics in the extended disk (additional data [27]). By subtracting the images acquired with and without  $I_{DC}$ , the dynamic response due to  $I_{DC}$  may be estimated (lower part of figure 2a). The subtracted images for the two in-plane (horizontal and vertical) channels each exhibit a spatially antisymmetric structure centred on the peak observed in the polar contrast, but occupying a somewhat larger area of  $\sim 2\mu\text{m}$  diameter. The subtraction yields negligible residual contrast in the extended region of the disk, confirming that the bullet mode is tightly confined at the centre of the disk.

Further measurements at different time delays [27] confirmed that the contrast in the magnetic channels oscillates with  $I_{RF}$ . However the contrast in the three

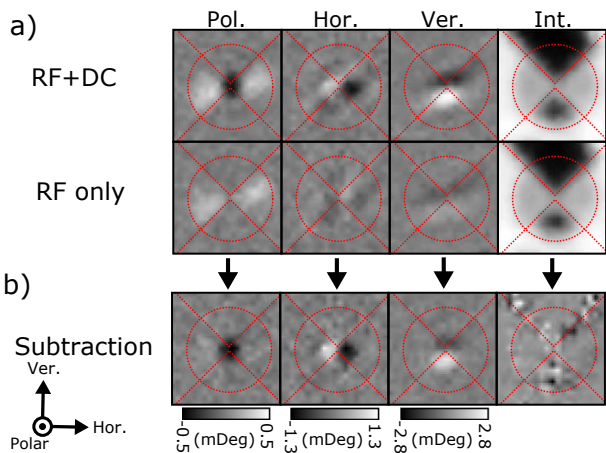


FIG. 2. a) TRSKM images acquired from the polar (out of plane), horizontal, vertical and reflected intensity channels of the vector bridge detector for a SHNO with  $d = 200$  nm,  $H = 650$  Oe,  $\theta_H = 210^\circ$ , and  $I_{RF} = 1.4$  mA at 6 GHz frequency.  $I_{DC} = 16$  mA and 0 mA in the upper and lower panels respectively. (b) The difference of the upper and lower images from (a) is shown, revealing contrast due to the presence of  $I_{DC}$  only. Each image shows a  $5 \mu\text{m}$  square region.

channels was observed to oscillate with the same relative phase, which is not expected if the magnetization undergoes a circular or elliptical precession. Furthermore, since  $H$  is applied  $30^\circ$  from the horizontal axis, the amplitude of the dynamic magnetization detected in the TRSKM experiment is expected to be significantly greater in the vertical as compared to the horizontal direction, while in fact these two components were found to have comparable amplitude. To aid interpretation of the experimental data, micromagnetic simulations were performed, using the MuMax 3 package after the current distribution and associated Oersted field had been calculated in COMSOL [27–29].

Images of the simulated bullet mode are presented in figures 3a for the configuration in figure 2. Initial simulations showed that the bullet quickly escapes the active area and is damped within the extended disk. Therefore a pinning site was introduced in the form of either a single cell discontinuity in the magnetization, or a localized 5% reduction in saturation magnetization with Gaussian spatial profile of  $\sim 240$  nm FWHM as in 3a. This led to a bullet mode that was stable for a finite range of  $I_{DC}$  values, as well as an additional mode that was localized in the non-uniform Oersted field associated with the injected charge current. The latter mode lies at higher frequency than the bullet mode, but was not observed in the room temperature electrical measurements of figure 1, and so not expected to appear in TRSKM measurements. Both the bullet and field-localized modes were found to have spatial and spectral character consistent with previous simulations [13, 14].

While the the bullet mode exhibits large angle pre-

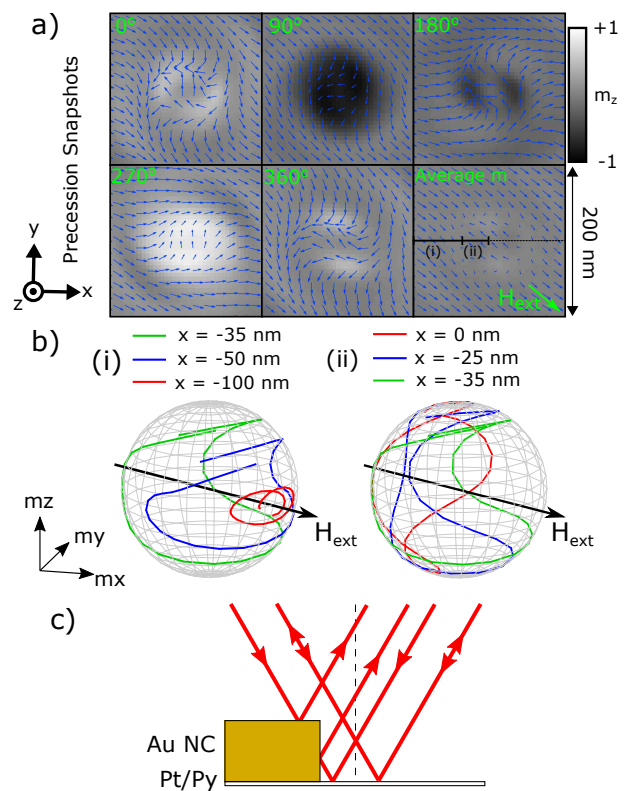


FIG. 3. a) Simulated magnetization profile at different phase values within the cycle of auto-oscillation. The arrows indicate the projection of the magnetization within the plane, while the grayscale represents the out of plane component. The images show the bullet mode with  $\sim 70$  nm diameter at the centre of the device. b) Trajectories of the magnetization for different points on the  $x$  axis, over 1 cycle of oscillation. c) Schematic to illustrate the artefact that generates contrast in the horizontal and vertical channels. Arrows indicate the direction of propagation of rays.

cession, the images in figure 3a do not reproduce the spatially antisymmetric character observed in the measured horizontal and vertical components. The core of the bullet mode undergoes the largest angle of precession. Figure 3b shows that outside the core region the magnetization undergoes elliptical precession about an axis parallel to the applied field. At the edge of the core region, at  $x = -35$  nm, the average magnetization is close to zero with an in-plane precession angle of  $\sim 270^\circ$ . Within the core the precession amplitude increases further so that the magnetization trajectory crosses over itself with the magnetization effectively precessing about a direction anti-parallel to the applied field. The magnetization precesses with the same phase at all positions within the disk. Simulations performed with an additional  $I_{RF}$  demonstrated slightly improved stability of the bullet, but otherwise the dynamics were of similar character.

Difference images, calculated from simulated images separated by  $180^\circ$  in phase, were convolved with a 870

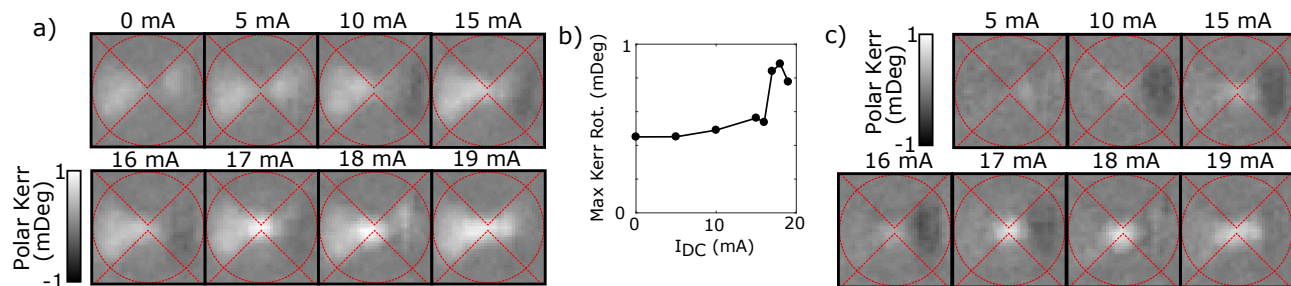


FIG. 4. a) Polar TRSKM images acquired for different  $I_{DC}$  values with the phase of  $I_{RF}$  fixed. b) Maximum absolute values of polar Kerr rotation extracted from the images in (a). (c) TRSKM images from (a) after subtraction of the  $I_{DC} = 0$  mA image. All images were recorded from a SHNO with  $d = 240$  nm, with  $I_{RF} = 0.8$  mA,  $H = 650$  Oe and  $\theta_H = 210^\circ$ .

nm full width half maximum Gaussian profile to more closely reproduce the experimental images. Again they did not reproduce the spatially antisymmetric contrast observed in the vertical and horizontal channels. Further tests showed that the antisymmetric contrast was observed only when the bullet mode was present, ruling out mechanisms such as polarization of the Pt by  $I_{RF}$  via the SHE. Therefore it was concluded that the in-plane contrast must be an artefact associated with the optical probe overlapping the edge of the 150 nm thick NCs, while in proximity to the bullet mode. Figure 3c provides a schematic representation of the likely mechanism. As the probe passes over the NCs the beam returning to the detector is partially obstructed. Crucially the symmetry between rays propagating in opposite directions within the cone is broken. The resulting difference in intensity of the two halves of the back-reflected beam, combined with a finite polar Kerr rotation due to the bullet mode, manifests as a signal similar to that due to the longitudinal MOKE from an in-plane component of magnetization[30]. It follows from the NC geometry that a top-bottom antisymmetry is observed in the vertical channel and a left-right antisymmetry in the horizontal channel.

The polar images are unaffected by the artefact. Figure 4a shows polar images acquired for different  $I_{DC}$  values, with the phase of  $I_{RF}$  fixed. The maximum absolute Kerr rotation was extracted from the images and plotted in figure 4b, while in figure 4c the images from 4a have been replotted after subtracting the image for which  $I_{DC} = 0$ . For small  $I_{DC}$  values the amplitude of the FMR mode increases gradually with increasing  $I_{DC}$  as the injection of DC spin current into the Py layer compensates the damping. For  $I_{DC} \geq 10$  mA a region of negative contrast appears to the right of the NCs. The asymmetry of the FMR response about the centre of the device reflects the mixed symmetry of the torques present. The STT and the torque due to the in-plane Oersted field are symmetric about the centre while the torque due to out of plane Oersted field is antisymmetric [26].

The microwave spectroscopy data of figure 1b revealed

the presence of a bullet mode for  $I_{DC} = 18 \rightarrow 20$  mA. However figure 4 shows strong out of plane dynamics at the NC tips for  $I_{DC} = 17$  mA, that is still present when  $I_{DC} = 19$  mA. The reduction of the threshold value for  $I_{DC}$  is due to the presence of the  $I_{RF}$ , as observed previously [10]. Figures 4a and c also demonstrate that the extent of localization of the bullet mode depends upon  $I_{DC}$ . Comparing the images for  $I_{DC} = 17 \rightarrow 19$  mA, the bullet mode is observed to occupy a larger region as  $I_{DC}$  is increased, with some reduction in the maximum Kerr amplitude. Since the diameter of this region is large compared to that of the bullet mode in figure 3a, this suggests that the bullet exhibits significant translational motion while being phase-locked to  $I_{RF}$ .

An optically-detected STT-FMR study of similar devices demonstrated a minimum in the torques at the centre of the device due to  $I_{RF}$  as a result of lateral current spreading. The bullet mode is therefore pulled towards where the STT is larger, and may either oscillate or gyrate about the centre. The bullet could either establish a stable trajectory, or escape and be damped in the extended disk [27], allowing another bullet to form at the centre and repeat the process. Increasing  $I_{DC}$  is likely to increase the mobility of the bullet, allowing it to move further from the centre. Since the linewidth of the microwave emission in 1b is only weakly dependent on  $I_{DC}$ , formation of a stable trajectory seems the more likely scenario.

In summary, time resolved images of the non-linear bullet mode within a SHNO have been obtained by stroboscopic TRSKM. The bullet was injection-locked to an RF current that simultaneously excites an FMR mode, but a simple subtraction procedure allows the contrast associated with the bullet to be isolated. While the out of plane component of the dynamic magnetization was unambiguously observed, the in-plane components were obscured by an artefact due to the edges of the thick electrical contacts. The localization of the bullet was found to decrease as the injected DC current was increased above the threshold value, and is attributed to spreading of the RF current from the centre of the device. Further work

is now required to determine the trajectory of the bullet within this more complicated torque landscape.

We acknowledge financial support from the Engineering and Physical Sciences Research Council (EPSRC) of the United Kingdom, via the EPSRC Centre for Doctoral Training in Metamaterials (Grant No. EP/L015331/1) and EPSRC grants EP/I038470/1 and EP/P008550/1.

- 
- [1] M. D. Stiles and J. Miltat, *Topics in Applied Physics* **101**, 225 (2006).
- [2] T. Jungwirth, J. Wunderlich, and K. Olejník, *Nature Materials* **11**, 382 (2012), arXiv:1411.3249v1.
- [3] A. V. Chumak, V. I. Vasyuchka, A. A. Serga, and B. Hillebrands, *Nature Physics* **11**, 453 (2015).
- [4] Y. K. Kato, R. C. Myers, a. C. Gossard, and D. D. Awschalom, *Science* **306**, 1910 (2004).
- [5] A. Hoffmann, *IEEE Transactions on Magnetism* **49**, 5172 (2013).
- [6] V. E. Demidov, S. Urazhdin, H. Ulrichs, V. Tiberkevich, A. Slavin, D. Baither, G. Schmitz, and S. O. Demokritov, *Nature Materials* **11**, 1028 (2012).
- [7] A. Brataas, A. D. Kent, and H. Ohno, *Nature Materials* **11**, 372 (2012).
- [8] R. Dumas, S. Sani, S. Mohseni, E. Iacocca, Y. Pogoryelov, P. Muduli, S. Chung, P. Durrenfeld, and J. Akerman, *IEEE Transactions on Magnetism* **50**, 1 (2014).
- [9] A. Hamadeh, O. d’Allivy Kelly, C. Hahn, H. Meley, R. Bernard, A. H. Molpeceres, V. V. Naleto, M. Viret, A. Anane, V. Cros, S. O. Demokritov, J. L. Prieto, M. Muñoz, G. de Loubens, and O. Klein, *Physical Review Letters* **113**, 197203 (2014), arXiv:1405.7415.
- [10] V. E. Demidov, H. Ulrichs, S. V. Gurevich, S. O. Demokritov, V. S. Tiberkevich, a. N. Slavin, A. Zholud, and S. Urazhdin, *Nature communications* **5**, 3179 (2014).
- [11] R. H. Liu, W. L. Lim, and S. Urazhdin, *Physical Review Letters* **110**, 147601 (2013).
- [12] M. Ranjbar, P. Durrenfeld, M. Haidar, E. Iacocca, M. Balinskiy, T. Q. Le, M. Fazlali, A. Houshang, A. A. Awad, R. K. Dumas, and J. Akerman, *IEEE Magnetism Letters* **5**, 1 (2014).
- [13] H. Ulrichs, V. E. Demidov, and S. O. Demokritov, *Applied Physics Letters* **104**, 042407 (2014).
- [14] A. Giordano, M. Carpentieri, A. Laudani, G. Gubbiotti, B. Azzerboni, and G. Finocchio, *Applied Physics Letters* **105**, 042412 (2014), arXiv:1407.7655.
- [15] V. E. Demidov, S. Urazhdin, A. Zholud, A. V. Sadovnikov, and S. O. Demokritov, *Applied Physics Letters* **105**, 172410 (2014).
- [16] A. A. Awad, P. Dürrenfeld, A. Houshang, M. Dvornik, E. Iacocca, R. K. Dumas, and J. Åkerman, *Nature Physics* **13**, 292 (2016).
- [17] T. Kendziorczyk and T. Kuhn, *Physical Review B - Condensed Matter and Materials Physics* **93**, 1 (2016).
- [18] H. Mazraati, S. Chung, A. Houshang, M. Dvornik, L. Piazza, F. Qejvanaj, S. Jiang, T. Q. Le, J. Weissenrieder, and J. Åkerman, *Applied Physics Letters* **109**, 242402 (2016).
- [19] M. Zahedinejad, A. A. Awad, P. Durrenfeld, A. Houshang, Y. Yin, P. K. Muduli, and J. Akerman, *IEEE Magnetism Letters* **8**, 1 (2017).
- [20] B. Divinskiy, V. E. Demidov, A. Kozhanov, A. B. Rinkevich, S. O. Demokritov, and S. Urazhdin, *Applied Physics Letters* **111** (2017), 10.1063/1.4993910.
- [21] P. Gangmei, P. S. Keatley, W. Yu, R. J. Hicken, M. a. Gubbins, P. J. Czoschke, and R. Lopusnik, *Applied Physics Letters* **99**, 2009 (2011).
- [22] R. A. J. Valkass, T. M. Spicer, E. Burgos Parra, R. J. Hicken, M. A. Bashir, M. A. Gubbins, P. J. Czoschke, and R. Lopusnik, *Journal of Applied Physics* **119**, 233903 (2016).
- [23] R. A. J. Valkass, T. M. Spicer, E. Burgos Parra, R. J. Hicken, M. A. Bashir, M. A. Gubbins, P. J. Czoschke, and R. Lopusnik, *Journal of Applied Physics* **119** (2016), 10.1063/1.4954018.
- [24] P. S. Keatley, S. R. Sani, G. Hrkac, S. M. Mohseni, P. Dürrenfeld, J. Åkerman, and R. J. Hicken, *Journal of Physics D: Applied Physics* **50**, 164003 (2017).
- [25] L. Liu, T. Moriyama, D. C. Ralph, and R. A. Buhrman, *Physical Review Letters* **106**, 036601 (2011).
- [26] As yet unpublished work under the title ‘Spatial Mapping of Torques within a Spin Hall Nano-oscillator’, TRSKM measurements on FMR.
- [27] See Supplemental Material at [URL tbc] containing additional injection locking data, and micro-magnetic results.
- [28] *Comsol 5.2a user manual*.
- [29] A. Vansteenkiste, J. Leliaert, M. Dvornik, M. Helsen, F. Garcia-Sanchez, and B. Van Waeyenberge, *AIP Advances* **4**, 107133 (2014), arXiv:1406.7635.
- [30] P. S. Keatley, V. V. Kruglyak, R. J. Hicken, J. R. Childress, and J. A. Katine, *Journal of Magnetism and Magnetic Materials* **306**, 298 (2006).